Available online at www.sciencedirect.com

ScienceDirect

journal homepage: www.elsevier.com/locate/burns

Tissue burns due to contact between a skin surface and highly conducting metallic media in the presence of inter-tissue boiling

John P. Abraham [a,*], John Stark [b], John Gorman [c], Ephraim Sparrow [c], W.J. Minkowycz [d]

[a] University of St. Thomas, School of Engineering, 2115 Summit Ave., St. Paul,MN 55105-1079, United States
[b] 3M Corporation, St. Paul, MN, United States
[c] University of Minnesota, Department of Mechanical Engineering, 111 Church St. SE, Minneapolis, MN 55455, United States
[d] University of Illinois at Chicago, Department of Mechanical and Industrial Engineering, 842 W. Taylor St., Chicago, IL 6060, United States

ARTICLE INFO

Article history:
Accepted 10 September 2018

Keywords:
Bioheat transfer
Contact burns
Hot surfaces
Burns
Thermal injury

ABSTRACT

A numerical-based model was developed and implemented to determine the spatial and temporal temperature distributions within skin tissue resulting from thermal contact with a heated and high thermal conductivity metallic medium. In the presence of wet tissue, boiling is likely to occur, thereby affecting the probability of inducing burns. This investigation deals with how contact between a hot, highly conductive metallic material and skin gives rise to burns. In particular, the study focuses on the likelihood that metals typically used in cooking or industrial applications may cause burns. Insofar as the surfaces under consideration are above the boiling temperature of water, a mathematical model including phase change was developed. That model allowed different thermophysical properties to be respectively employed for dry and wet tissues.

Multiple processes and their governing parameters were investigated to assess their impact on burn severity, including the temperature of the metal, the duration of contact, the contact resistance between the surface and the skin, the temperature range over which phase change occurred, and the cooling environment after the exposure. It was discovered that the most important parameters are the surface temperature and exposure duration. The other conditions/parameters had lesser impacts on the results.

1. Introduction

Skin burns are a very common form of thermal injury which occur ubiquitously around the globe. Typical causes of thermal burns include contact with hot liquids (scald burns), direct contact with heated solid materials (contact burns), radiant heating, or direct contact with flames or hot gases.

There is a rich literature on skin burns due to each of these causes. However, since the present focus deals with contact involving skin and elevated-temperature metallic media, literature specific to that situation will be featured here.

* Corresponding author.
E-mail address: jpabraham@stthomas.edu (J.P. Abraham).
https://doi.org/10.1016/j.burns.2018.09.010

However, readers seeking a broader exposure to skin burns in general are directed to references [1–15].

To the best knowledge of the authors, the seminal papers dealing with contact burns are conveyed in [16–18] which collectively cover both experimental and numerical modeling works. These references are excellent starting points, but they correspond to temperatures which are significantly below those which may be experienced in a real-life situation, such as during cooking. Furthermore, these lower temperature studies deal with long exposures (~5s, for instance, in [18]) which is longer than an actual exposure may be.

Therefore, it is the goal of this study to extend the range of knowledge to higher temperature exposures of shorter duration. In fact, the exposure temperatures are guided by typical cooking temperatures (~225°C, ~440F) and for exposures of 2s or less.

Included in the investigation is the accounting of contact resistance between the skin and the metal medium and the effect of inter-tissue phase change (boiling) on the thermal wave within the tissue.

2. Heat transfer and burn model

2.1. *The geometrical model*

The physical situation and the contact process is illustrated in a simplified schematic drawing in Fig. 1. The tissue approaches the conductive surface, remains in contact with the surface for some time period, and then is withdrawn. The exposure period is determined by the reflex response of the person, typically on the order of 1s.

In the present study, no preheating is considered, nor is post-contact heating. While there may be some small amount of pre- and post-heating caused principally by radiant heat transfer, this effect will be negligible. Consequently, the heat transfer processes that are modeled are during the tissue-surface contact period and shortly afterwards. After the tissue has been separated from the hot surface, convection to an external environment occurs. The external environment is assumed to be at 20°C with an effective convection/radiation heat transfer coefficient of 10W/m^{2}K. This value is typical of simultaneous convection and radiation processes; however, the outcome of the calculations is not sensitive to the post-heating thermal conditions. In fact, applying a convective coefficient of zero W/m^{2}K gave results that were nearly indistinguishable from the aforementioned ambient conditions. The basis for this finding is that the heat transfer processes after the exposure are dominated by conduction within the tissue, convective/radiative losses are very minor.

During contact, the situation is shown in enlarged view in Fig. 2. As shown there, the thickness of the conductive material is selected to be greater than three mm. That thickness was found to be effectively infinitely thick [18]. In fact, materials thinner than three mm behaved approximately as infinitely thick. This behavior is a consequence of the large product of thermal capacity and conductivity of the highly conducting materials (compared with skin) and the relatively short durations of contact.

Initial two-dimensional calculations were performed that enabled both perpendicular and transverse heating, as shown in Fig. 3. That figure is an illustrative schematic which shows, by colors, a heat wave penetrating the tissue. It was discovered that the lateral heat wave traveled a much shorter distance than did the perpendicular wave. Consequently, the results were essentially one-dimensional, even for small-sized hot surfaces (on the order of one cm width). Consequently, two-dimensional calculations were abandoned when found to be unnecessary.

2.2. *The mathematical model*

Heat transfer within the tissue is modeled using the classic Pennes bioheat equation [18], expressed as

$$(\rho c_p)_t \frac{\partial T_t}{\partial t} = k_t \frac{\partial^2 T_t}{\partial x^2} + \omega(\rho c_p)_b (T_b - T_t) \quad (1)$$

which is used to calculate temperatures at all locations and times during the exposure and post-exposure cooling. The first term on the left reflects the unsteady temperature variation within the tissue. The second term represents conduction through the tissue. The third term is the effect of blood perfusion. The symbols ρ, c_p, and k are the density, specific heat, and thermal conductivity, respectively. The symbol T is

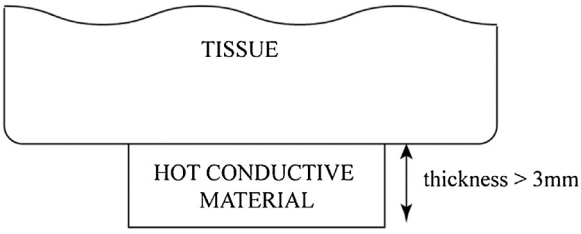

Fig. 2 – The geometry associated with tissue-surface contact.

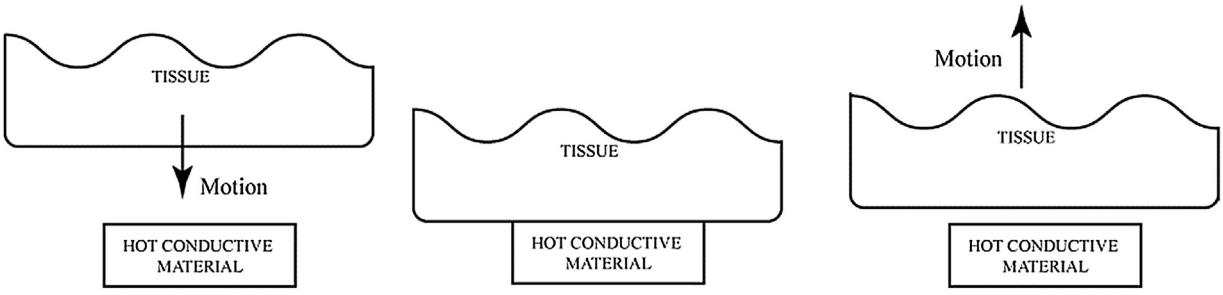

Fig. 1 – Simplified schematic diagram of the contact process.

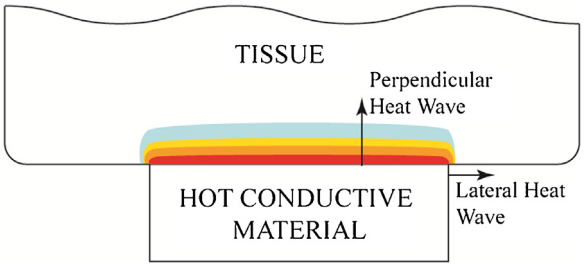

Fig. 3 – Schematic illustration showing relative perpendicular and lateral heat penetration.

local temperature. The subscripts *t* and *b* correspond to tissue and blood, respectively. The symbol ω is the local volumetric blood perfusion term. There is also a heat source term from metabolism but that is much too small to matter in the short time period of the heating and cooling after the exposure. The temperatures obtained by solving Eq. (1) are incorporated into an injury metric model obtained from [19–22] which is

$$\Omega(x,t) = \xi \int_0^t e^{-\left(\frac{\Delta E}{RT}\right)} d\lambda \tag{2}$$

Here, R is the ideal gas constant, *T* is the local temperature in absolute units, λ is a variable of integration, and Ω is the injury metric. The symbols ξ and ΔE represent tissue-specific injury parameters which have been determined by experimentation. The values of these parameters obtained from [19–22] are ξ=3.1e98 (1/s) and ΔE=6.28e8 (J/kmol). While other researchers have offered variations to these injury parameters, the values presented here are still most-often used and considered a gold-standard with a history of demonstrated accuracy for skin-burn predictions. Permanent local injury has occurred when the value of Ω=1. This metric has been used extensively with success for many bioheat transfer problems and is adopted here.

2.3. *Tissue thermophysical properties*

The metal temperatures will give rise to values exceeding those which cause liquid-vapor phase change. Consequently, inclusion of the energy required to cause phase change, as well as the material properties for dry and wet skin must be made. Table 1 provides a listing of the material properties used in the model. For all tissue layers, the value of perfusion is 0.00125 1/s [12]. It turns out that the results are not sensitive to the value of the perfusion rate because local heat loss to perfusing blood is much lower than heat transfer from the metal contact surface and conduction within the tissue. The tissue is a three-layer model with an epidermis layer (0.08 mm), a dermal component (2 mm), and a subcutaneous fat layer (10 mm), as indicated in the table.

The thermal conductivity values are reduced by the percentage of water which is initially within the tissue (~50% for epidermis and 70% for dermis) [23]. While the thermal conductivity is a transport property rather than a thermodynamic property, it has been found that thermal conductivity varies linearly with water content [24–29].

The justification for the changes to heat capacity are based on the percentage of water in the respective regions. As local temperatures rise from 95 to 105 °C, the intracellular water will evaporate and consequently, the product ρc_p must change to reflect this phase change. Since it is the product of these two quantities that matters; both the density and heat capacity of the epidermis decrease by ~50% as inter-tissue water evaporates, such that the decrease in the product of the two is a factor of ~4. For the decrease in ρc_p in the dermal layer, information from [28] was used.

As indicated in Table 1, phase change occurs between temperatures of 95 and 105 °C. The heat capacity within that region is taken to be the heat of fusion divided by the temperature range over which evaporation occurs. A sensitivity study was carried out using different evaporation temperature ranges of 2.5 °C, 5 °C, and the 10 °C value listed in the table. For an evaporation range of 2.5 °C, it was assumed that inter-tissue water evaporated as the tissue heated from 97.5 to 100 °C. For the 5 °C evaporation range, it was assumed that the inter-tissue liquid water evaporated as the tissue heated from 95 °C to 100 °C. The final results were virtually indistinguishable from each other, regardless of the temperature range over which the evaporation occurred.

2.4. *Thermal boundary conditions*

Contact between two initially isothermal objects can give rise to an interface temperature which has a theoretical expression of:

$$T_{interface} = \frac{T_1\sqrt{(\rho c_p k)_1} + T_2\sqrt{(\rho c_p k)_2}}{\sqrt{(\rho c_p k)_1} + \sqrt{(\rho c_p k)_2}} \tag{3}$$

Table 1 – Summary of thermophysical properties used in the calculations.

Layer	Thermal Conductivity, *k* (W/mK)	Density, ρ (kg/m^3)	Specific Heat, c_p (J/kgK)	Temperature Range
Epidermis	0.22	1200	3600	T < 95 °C
	Linear variation		113,000	95 °C < T < 105 °C
	0.11		900	T > 105 °C
Dermis	0.4	1200	3600	T < 95 °C
	Linear variation		158,000	95 °C < T < 105 °C
	0.12		440	T > 105 °C
Subcutaneous	0.2	900	2500	All temperatures

where subscripts 1 and 2 denote the two dissimilar materials. It was decided to forego this analytical treatment for numerous reasons. First, it is assumed that there exists perfect thermal contact between the two materials which could not happen in practice. Second, it neglects phase change processes which will occur at the temperatures of the present study. Third, the product $\rho c_p k$ for metals is much larger than that of the epidermis so from a practical standpoint, the interface temperature would be close to that of the metal.

To account for the above-mentioned issues, it was decided to treat the metal as an isothermal volume (temperature constant in time) which exchanges heat with the epidermal surface through a contact conductance $h_{contact}$, so that the surface flux condition becomes

$$q''_{surf} = h_{contact}\left(T_{metal} - T_{epidermis,surf}\right) \quad \text{for} \quad t < t_{exposuret} \tag{4}$$

Here, $q''_{surf}$is the surface heat flux, $h_{contact}$ is a contact conductance during the thermal exposure, T_{metal} is the temperature of the highly-conducting metal, and $T_{epidermis,surf}$ is the temperature of the epidermal surface. After the conclusion of the exposure time, the following boundary condition is used

$$q''_{surf} = h_{eff}\left(T_{amb} - T_{epidermis,surf}\right) \text{ for } t < t_{exposure} \tag{5}$$

As noted earlier, h_{eff}=10W/m^{2}K and T_{amb}=20°C.

To the best knowledge of the authors, there is no information on the values of contact conductance between tissue and metallic surfaces. It is known that the values would depend strongly on the interfacial pressure and the flatness and roughness of both surfaces. Consequently, the value of $h_{contact}$ was systematically increased until further increases did not change the resulting temperatures within the epidermis. It was found that when values of $h_{contact}$ exceeded 5000W/m^2°C, temperature results changed by at most 2%. For the final calculations, a value of $h_{contact}$=9000W/m^2°C was used. To further verify that the selected value was sufficiently high, calculations were carried out using $h_{contact}$ as high as 100,000W/m^2°C. Timewise temperature variations at the dermal/epidermal interface were within 1°C of those obtained when $h_{contact}$=9000W/m^2°C was used.

The deep-tissue condition (inner temperature of fat surface) of 37°C was employed. This surface was far enough from the heating zone so that its impact did not affect the results.

The initial temperature throughout the tissue was set to the body core temperature of 37°C. In reality, the temperature is slightly lower in the epidermis; however, the difference is negligible, particularly compared to the rapid rise in epidermis temperatures upon contact with the highly conductive material.

The computations were performed using a control-volume approach with ANSYS CFX v 18.0. Ten elements were deployed in the epidermal layer, 30 in the dermal layer, and 30 in the fat layer. The elements were deployed so that they grew in size for deeper-tissue locations.

The unsteady calculations required timewise integration which was carried out with time steps that varied between 0.01–1e-6 s. The computational mesh and time step values were a consequence of a mesh- and time-step independence study so that all results are independent of the size of the elements and time steps.

As an example of mesh and time step independency, Fig. 4 has been prepared. That figure shows temperature results at the epidermal surface and at the epidermis/dermis interface. The temperatures correspond to a metal temperature of 150C and a contact duration of 1s. Each location is characterized by two different-colored curves. One of the curves pertains to the a time step of 0.001s and the element sizes discussed above. The other curves correspond to time steps of 0.0005 s and twice the element count. It is seen that the results are indistinguishable. Similar images could be created for other test cases by they are not shown here for sake of brevity.

While the calculations will be discussed in greater detail later in the manuscript, the changes to slope in the

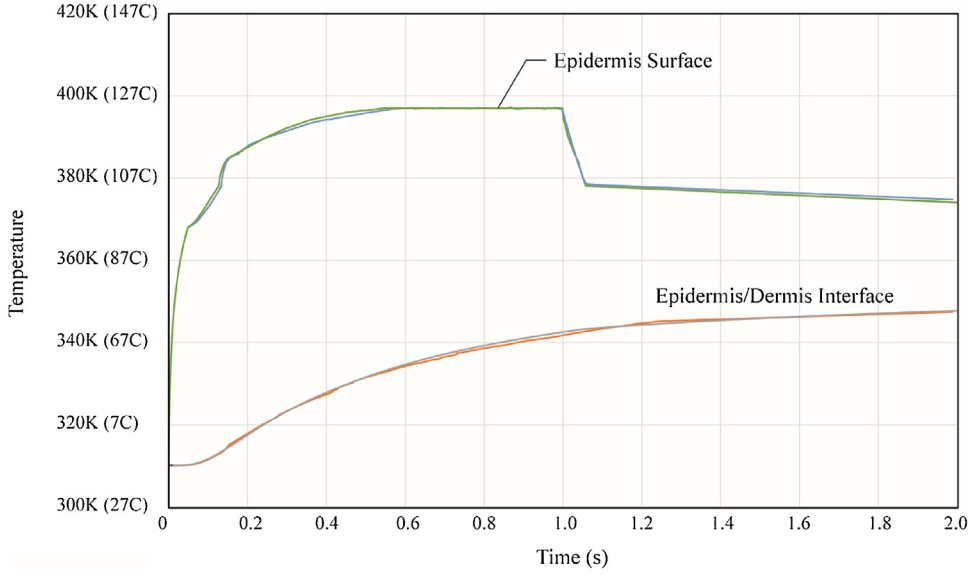

Fig. 4 – Epidermal and dermis/epidermis interface temperatures, demonstrating mesh and time-step independency).

epidermal temperature curve at approximately 95C and 105C are related to the onset and cessation of boiling. At one second, the temperature at the epidermis surface decreases quickly and thereafter much more slowly because the epidermis is again in a phase-change region (after approximately 1.05s) wherein water is recondensing. The recondensation is still ongoing at the 2s time period and is characterized by a nearly constant temperature at the epidermis. Deeper in the tissue, the temperature response is quite different. There is a slow and gradual rise in temperature, at no point are temperatures hot enough so that phase change is activated. However, the temperatures are still rising slowly at the two-second time, even though the epidermis surface is cooling. Much more detailed regarding tissue temperature behaviors will be provided in the following section.

Table 2 – List of calculation parameters.

Metal Temperature (°C)	Exposure Duration (s)	Nomenclature
150	0.5	Case 1, exposure 0.5s
	1	Case 1, exposure 1s
	2	Case 1, exposure 2s
175	0.5	Case 2, exposure 0.5s
	1	Case 2, exposure 1s
	2	Case 2, exposure 2s
200	0.5	Case 3, exposure 0.5s
	1	Case 3, exposure 1s
	2	Case 3, exposure 2s
225	0.5	Case 4, exposure 0.5s
	1	Case 4, exposure 1s
	2	Case 4, exposure 2s

3. Results and discussion

With the use of the information from the preceding section, results from the calculations can now be presented. The calculations utilized multiple metal temperatures and exposure durations, as listed in Table 2. For each simulation, the calculations were continued after the exposure, until temperatures within the entirety of the tissue had reached values that would no longer cause thermal injury (below 43°C).

3.1. *Evaluating the numerical model*

When presenting the results from a numerical model, it is important to provide validation to ensure that the model correctly captures the governing phenomena of the problem and provides accurate results. A discussion of the accuracy of the numerical model will now be provided. It is noteworthy that the model utilized in this investigation is that of [12–15] which was compared there to multiple physical observations of scald injuries. While those scald injuries were caused by temperatures that were not sufficiently high to cause inter-tissue evaporation, they do, nevertheless, provide a partial test of the underlying algorithm.

A comparison of the observations will now be provided as set forth in Fig. 5. A similar comparison was made in [12] using data from references [2,16,21,30–33] and the same references are used here. While the experiments did not provide measured burn depths, the injury extents were made by medical observation. The references corresponded to skin heating from exposure to hot liquids. Nevertheless, the physical processes involved in that heat transfer problem are very similar to heat transfer into skin from a hot surface.

Fig. 5 is provided that shows results obtained using the current algorithm. Any temperature-time combinations above the line corresponds to deep partial thickness (or greater) burns. Any temperature-time combinations below the lowermost line corresponds to superficial partial thickness burns or less. It is seen that all experimentally obtained superficial partial thickness burns (indicated by triangles) are below the

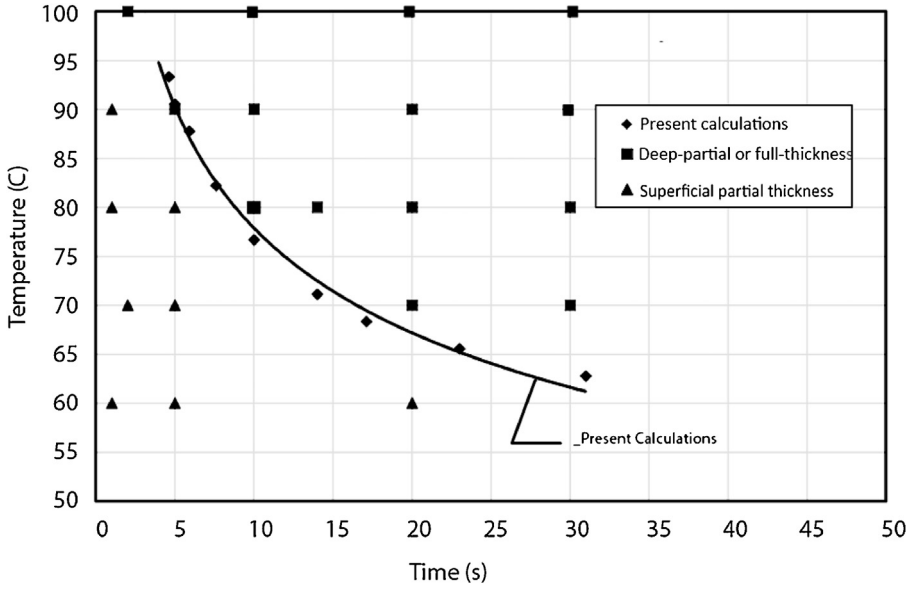

Fig. 5 – Comparison of present calculation method against physical observations of burn depths.

predictions of the model. It is also seen that all deep-partial or full-thickness burns from the observations (signified by square) are above the prediction line of the model (22 out of 22 cases correctly predicted).

In addition, when the present model is applied to compare with the results from [18], it is found that the "safe touch temperature" reported in [18] is ~56°C while here 58°C was found. In making this comparison, we adopted the definition of "safe touch" provided in [18], that is, the interface location incurred an injury of $0.45 < \Omega < 0.5$ for an exposure duration of 5s. Not only are these temperature results (56°C and 58°C) in excellent agreement but the slight difference is expected because [18] used a theoretically perfect contact between the skin and the metal surface. The inclusion of a contact resistance in the current algorithm results in an interface temperature difference between the metal and skin surface of ~2°C. That is, in the present calculations, contact between a 58°C metal resulted in a maximum epidermal temperature of 56°C (in perfect agreement with [18]).

With the underlying algorithm evaluated, attention is turned to the sensitivity of the evaporation model. As discussed earlier, the evaporation model assumes that the latent heat related to phase change of liquid water to water vapor is released/absorbed over a finite temperature range. The width of that range determines the effective tissue heat capacity. To the best knowledge of the authors, there is no available information that can be definitively relied upon to ascertain the temperature range over which intertissue boiling occurs. To deal with this uncertainty, calculations were completed for different evaporation ranges of 2.5, 5, and 10°C. The test case from Table 2 was Case 4, with a one-second exposure. With this scenario, the spatial temperature variation within the tissue was extracted at both 1 and 2s after the initial contact. The temperature variations at the 1- second mark (at the end of the skin-metal exposure) are shown in Fig. 6. It can be seen from the main part of the figure as well as from the expanded figure that focuses on the first 0.5mm of tissue, there is virtually no difference in the outcome. That is, regardless of the evaporation range that was selected, the results were nearly identical. It appears that that salient feature is that the evaporation model allows the entirety of the required energy for phase change to be accounted for. Similarly, in Fig. 7, it can be seen that at the 2-second time (2s after initial contact with the hot surface), the temperature variations are still in excellent agreement, regardless of the value of the phase change range.

Regardless of the temperature range over which liquid water was allowed to evaporate, the mathematical model included the entirety of the latent heat capacity of the water. It is apparent then, from Figs. 6 and 7, that the important issue is that the entire latent heat capacity was included, but it is not very important if that latent heat was absorbed/liberated over a 10°C range, or another temperature range.

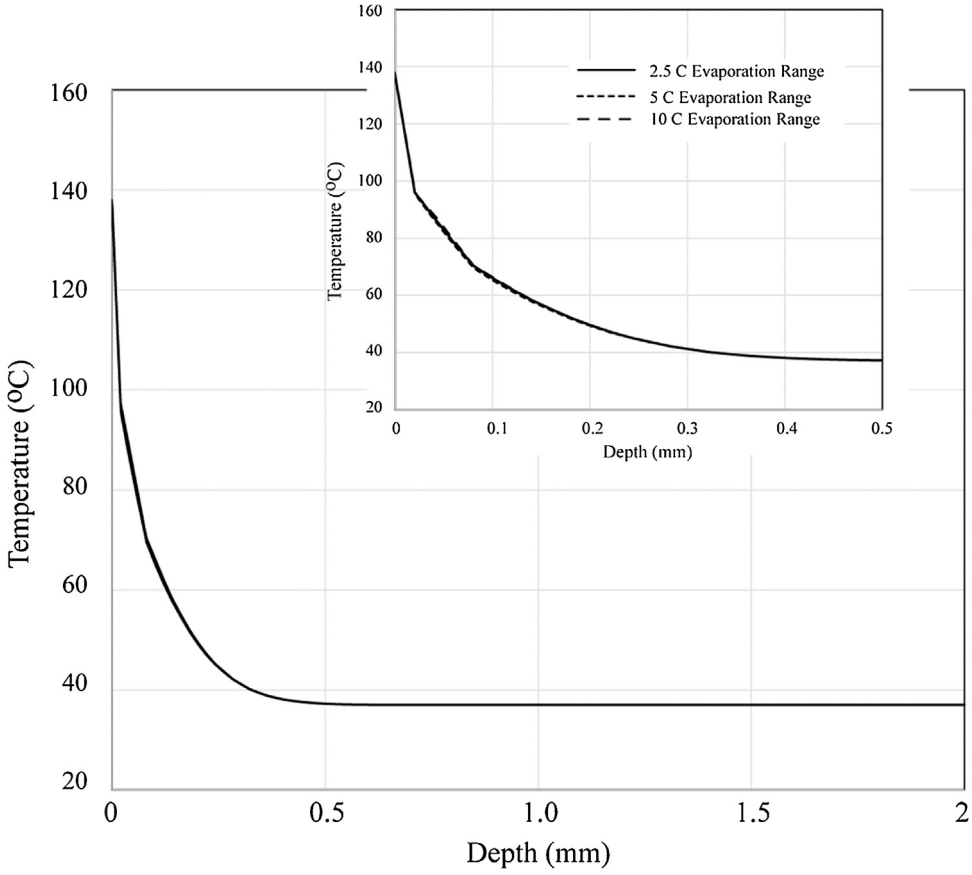

Fig. 6 – Spatial variation of temperature within the tissue for three different evaporation ranges, results correspond to Case 4 (surface temperature = 225°C) and an exposure time of 1 s. The temperature variations are extracted at the 1-second mark, which coincides with the cessation of the exposure.

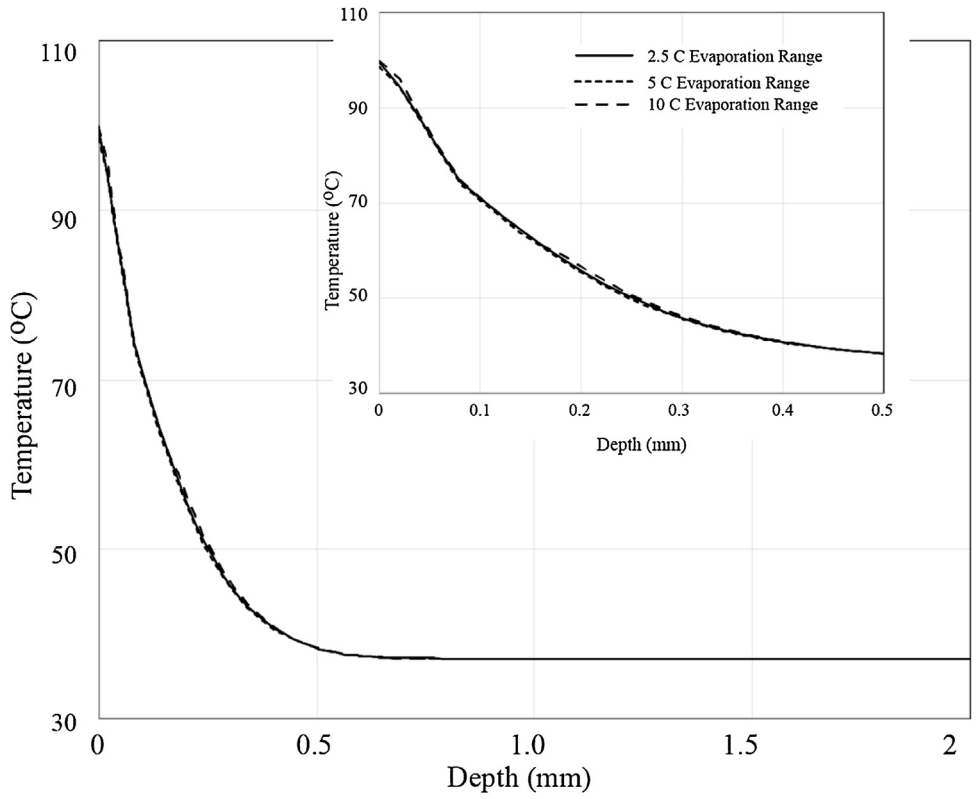

Fig. 7 – Spatial variation of temperature within the tissue for three different evaporation ranges, results correspond to Case 4 (surface temperature=225°C) and an exposure time of 1s. The temperature variations are extracted at the 2-second mark (1-second after the cessation of heating).

3.2. *New results for skin contact with high-temperature surfaces*

With the issues of model accuracy dealt with, attention is now turned to the presentation of results that are the specific focus of this study and, to the best knowledge of the authors, not conveyed in other prior literature. First, temperature results are provided at a multitude of locations within the tissue. Since the various cases all demonstrate similar qualitative behavior, only a subset of temperatures from Table 2 will be displayed.

First, results for Case 1 with a 0.5-second exposure are shown in Fig. 8. The figure shows that the exposure surface of the epidermis reaches very high temperatures quickly and then the temperature there decreases after the hot surface is removed from contact with the skin. Temperatures deeper in the skin rise slower and continue to rise long after the initial exposure. At deeper locations, not only is the peak temperature much lower compared to the skin surface, but also, the peak occurs at much later times – well after the epidermis temperature has declined. The only location which displays the characteristics of phase change is the

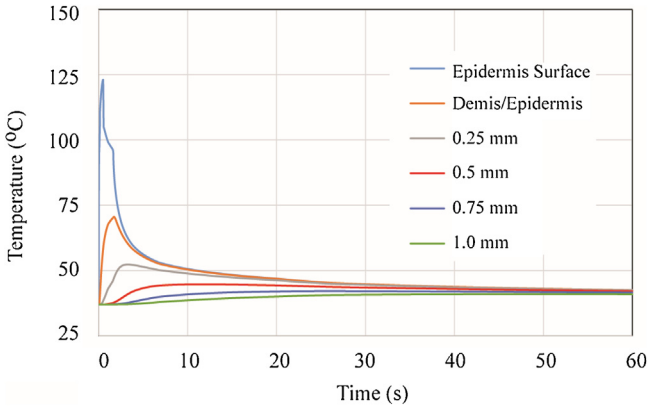

Fig. 8 – Case 1, 0.5s exposure, temperature variations at multiple locations within tissue.

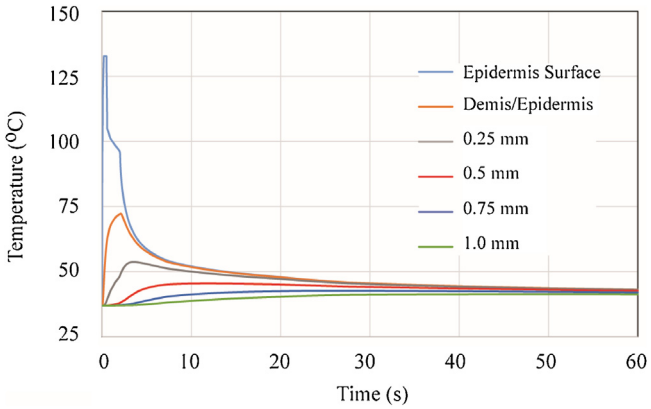

Fig. 9 – Case 2, 0.5 s exposure, temperature variations at multiple locations within tissue.

epidermis. There, a maximum temperature of ~123C is reached very quickly. This is followed by a very rapid cooling after the hot metal is removed. It should be noted the phase change occurs in two stages. First, during the heating, evaporation occurs. Then, condensation occurs while the tissue cools to the 95–105 °C range. In the image, the effect of evaporation cannot be seen because it occurs so quickly; however, the condensation is clearly evident. At approximately 2.5 s, there is a noticeable change in the slope of the epidermis temperature. This change in slope coincides with the cessation of condensation.

Next, Case 2 results with a 0.5-second exposure are shown in Fig. 9. Again, it is seen that the temperatures near the epidermal surface rise very rapidly during the exposure and then fall rapidly after the contact. Temperatures within the tissue rise slower and reach their peak values sometime after the initial exposure. As noted with the prior figure, the temperatures at progressively deeper locations reach their maximum values later and they exhibit a much more gradual rise and decline compared to the epidermal surface. Also noteworthy is the clear effect of phase change which is evident in the epidermal temperatures. When the temperatures are within the 95–105 °C range, the timewise temperature change is slow. However, when the epidermis temperature is greater than 105 °C or less than 95 °C, its temperature changes much more quickly – a consequence of the latent heat capacity of water as it changes phase.

Displayed in Fig. 10 are the temperatures corresponding to Case 4 temperatures and a 0.5- second exposure. As seen earlier, the temperatures deeper within the skin rise slowly and continue to rise long after the initial thermal insult.

The earlier observations in connection with Figs. 8 and 9 are also evident in Fig. 10, and are not repeated.

The listing in Table 3 summarizes the maximum dermal temperatures (at the interface between the dermis and the epidermis) for the various cases in Table 2. This location was selected because of its importance in determining the state of injury at this location. When the interface between the dermis and the epidermis has experienced thermal necrosis, the burn has transitioned from *superficial* to either *superficial partial thickness* or *deep partial thickness* (from first degree to either second or third degree).

Next, timewise temperatures variations were extracted at various locations within the tissue layers and these temperatures were employed for the calculation of the thermal injury using Eq. (2). The results are displayed in Tables 4a–4d. While it is evident that both longer exposure durations and higher surface temperatures give rise to injury that extends deeper into the tissue, in none of the cases does irreversible injury extend to 0.5 mm depths or greater. However, the burn injuries

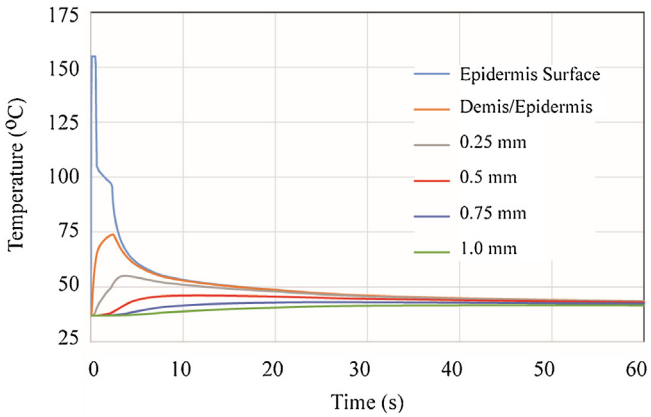

Fig. 10 – Case 4, 0.5 s exposure, temperature variations at multiple locations within tissue.

Table 3 – Summary of maximum epidermal temperature.

Metal Temperature (°C)	Exposure Duration (s)	Maximum Dermal Temperature (°C)
150	0.5	70.6
	1	77.3
	2	82.4
175	0.5	72.4
	1	78.0
	2	82.6
200	0.5	73.2
	1	78.3
	2	83.1
225	0.5	74.1
	1	78.6
	2	83.5

Table 4a – Injury results (Ω) corresponding to Case 1 (Metal temperature = 150 °C). Ω values in excess of 1 indicates permanent and irreversible damage.

	Exposure Duration (s)		
Location	0.5	1	2
Top Epidermis	5.9×10^{14}	2.4×10^{15}	4.0×10^{15}
Dermis/Epidermis interface	650	9.8×10^{4}	4.2×10^{6}
0.25 mm	0.019	1.2	110
0.5 mm	0	0.005	0.09
0.75 mm	0	0.001	0.005

Table 4b – Injury results (Ω) corresponding to Case 2 (Metal temperature = 175 °C). Ω values in excess of 1 indicates permanent and irreversible damage.

	Exposure Duration (s)		
Location	0.5	1	2
Top Epidermis	1.6×10^{17}	4.0×10^{17}	8.9×10^{17}
Dermis/Epidermis interface	2600	1.7×10^{5}	5.7×10^{6}
0.25 mm	0.046	2.2	150
0.5 mm	0.001	0.007	0.11
0.75 mm	0	0.001	0.006

Table 4c – Injury results (Ω) corresponding to Case 3 (Metal temperature = 200 °C). Ω values in excess of 1 indicates permanent and irreversible damage.

	Exposure Duration (s)		
Location	0.5	1	2
Top Epidermis	1.7×10^{19}	3.8×10^{19}	1.2×10^{20}
Dermis/Epidermis interface	4600	2.2×10^{5}	8.3×10^{6}
0.25 mm	0.065	2.6	240
0.5 mm	0.001	0.008	0.14
0.75 mm	0	0.001	0.008

Table 4d – Injury results (Ω) corresponding to Case 4 (Metal temperature = 225 °C). Ω values in excess of 1 indicates permanent and irreversible damage.

	Exposure Duration (s)		
Location	0.5	1	2
Top Epidermis	6.9×10^{20}	1.2×10^{21}	1.3×10^{21}
Dermis/Epidermis interface	7900	2.7×10^{5}	1.1×10^{7}
0.25 mm	0.11	3.5	360
0.5 mm	0.001	0.009	0.19
0.75 mm	0	0.001	0.010

do extend into the dermal layer and are, therefore, considered second-degree burns.

It should be noted that while the calculations here were performed direct contact burns, the modeling can also be used for other, intentional heating procedures such as intentional hyperthermia, and the use of elevated temperature to increase inter-tissue mass transport. As such, the analysis can be incorporated in other research ventures, such as [34,35].

4. Concluding remarks

A numerical model was developed and implemented to determine the spatial and temporal temperature variations within skin tissue after exposure to a heated and high thermal conductivity metallic material. The impact of various parameters was assessed, including the time of exposure and the temperature of the heated surface. Since the temperatures of the heated surfaces were sufficiently high to cause liquid-vapor phase change, the impact of this phenomena was included.

The model was tested against prior research and found to be in excellent agreement. The novel feature here, which is not present in the prior art, is the inclusion of phase change. To determine whether the means of treating phase change impacted the results, three different scenarios were simulated which had different evaporation range temperatures. It was discovered that the results were indistinguishable from each other.

For the cases considered here, which are typical of temperatures that may be experienced with cooking, burn injuries extended well into the dermal layer but did not pass the mid-plane of the dermis. Consequently, these types of exposures are properly classified as *superficial partial thickness* burns. The results presented here are limited to the temperatures and exposure durations investigated. Care should be exercised before extrapolating these findings beyond the investigated ranges of the parameters.

Conflict of interest

Professor Abraham has served as an expert witness in scald injury litigation.

Acknowledgements

No funding for this study.

REFERENCES

[1] Abraham JP, Nelson-Cheeseman BB, Sparrow EM, Wentz JE, Gorman JM, Wolf SE. Comprehensive method to predict and quantify scald burns from beverage spills. Int J Hyperthermia 2016;32:900–10.
[2] Diller KR. Modeling thermal skin burns on a personal computer. J Burn Care Rehab 1998;19:420–9.
[3] Ng EYK, Tan HM, Ooi EH. Boundary element method with bioheat equation for skin burn injury. Burns 2009;35:987–97.
[4] Ng EYK, Chua LT. Prediction of skin burn injury. Part 1: numerical modeling. J Eng Med 2002;216:157–70.
[5] Ng EYK, Chua LT. Prediction of skin burn injury: Part 2: parametric and sensitivity analysis. J Eng Med 2002;216:171–83.
[6] Ng EYK, Chua LT. Comparison of one- and two-dimensional programmes for predicting the state of skin burns. Burns 2002;28:27–34.
[7] Dai W, Wang H, Jordan PM, Mickens RE, Bejan A. A mathematical model for skin burn injury induced by radiation heating. Int J Heat Mass Transf 2008;51:5497–510.
[8] Ross DC, Diller KR. An experimental investigation of burn injury in living tissue. J Heat Transfer 1976;98:292–6.
[9] Torvi DA, Dale JD. A finite element model of skin subjected to a flash fire. J Biomech Eng 1994;116:250–5.
[10] Diller KR. Modeling of bioheat transfer processes at high and low temperature. Advances in heat transfer. . p. vol. 22.
[11] Abraham JP, Plourde BD, Vallez LJ, Nelson-Cheeseman BB. Correcting a prevalent misunderstanding of burns. Burns 2016;42:715–6.
[12] Abraham JP, Plourde BD, Vallez LJ, Stark JR, Diller KR. Estimating the time and temperature relationship for causation of deep-partial thickness skin burns. Burns 2015;41:1741–7.
[13] Viglianti BL, Dewhirst MW, Gorman JM, Abraham JP, Sparrow EM. Rationalization of thermal injury quantification methods: application to skin burns. Burns 2014;40:896–902.
[14] Johnson NN, Abraham JP, Helgeson ZI, Minkowycz WJ, Sparrow EM. An archive of skin-layer thicknesses and properties and calculations of scald burns with comparisons to experimental observations. J Therm Sci Eng Appl 20113: 011003.
[15] Ye H, De S. Thermal injust of skin and subcutaneous tissues: a review of experimental approaches and numerical models. Burns 2017;43:909–32.
[16] Diller KR, Hayes LJ, Blake GK. Analysis of alternate models for simulating thermal burns. J Burn Care Rehab 1991;12:177–89.
[17] Lawrence JC, Bull JP. Thermal conditions which cause skin burns. Eng Med 1976;5:61–3.
[18] Subramanian B, Chato JC. Safe touch temperatures for hot plates. J Biomech Eng 1998;120:727–36.
[19] Pennes HH. Analysis of tissue and arterial blood temperatures in resting human forearm. J Appl Physiol 1948;1:93–133.
[20] Moritz AR, Henriques FC. Studies of thermal injury I. The conduction of heat to and through the skin and the temperature attained therein. Am J Pathol 1947;23:531–49.
[21] Moritz AR, Henriques FC. Studies of thermal injury II. The relative importance of time and surface temperature in the causation of cutaneous burns. Am J Pathol 1947;23:695–720.
[22] Moritz AR. 1947, Studies of thermal injury III. The pathology and pathogenesis of cutaneous burns, an experimental study. Am J Pathol 1947;23:915–41.
[23] Henriquez FC. 1947, Study of thermal injury V. The predictability and significance of thermal induced rate processes leading to irreversible epidermal injury. Arch Pathol 1947;43:489–502.
[24] Guzman-Alonso M, Cortazar TM. Water content at different skin depths. Dermatology 2016;11:35–40.
[25] Duck FA. Physical Properties of Tissue, a Comprehensive Reference Book. London: Academic Press; 1990.
[26] Cooper TE, Trezek GJ. Correlation of thermal properties of some human tissues with water content. Aerospace Med 1971;42:24–8.
[27] Sweat VE. Modeling the thermal conductivity of meats. Trans ASAE 1975;18:564–8.
[28] Spells K. The thermal conductivities of some biological fluids. Phys Med Biol 1960;5:139–52.
[29] Abraham JP, Sparrow EM. A thermal ablation model including liquid-to-vapor phase change, necrosis-dependent perfusion, and moisture-dependent properties. Int J Heat Mass Transf 2007;50:2537–44.
[30] Singer AJ, Berutti L, Thode HC, McClain SA. Standardized burn model using multiparametric histologic analysis of burn depth. Acad Emerg Med 2000;7:1–6.
[31] Torvi DA, Threlfall TG. Heat transfer model of flame resistant fabrics during cooling after exposure to fire. Fire Technol 2006;42:27–48.
[32] Knabl JS, et al. Controlled partial thickness burns: an animal model for studies of burn wound progression. Burns 1999;25:229–35.
[33] Jiang S, Ma N, Li H, Zhang X. effects of thermal properties and geometrical dimensions on skin burn injuries. Burns 2002;28:713–7.
[34] Mahjoob S, Vafai K. Analytical characterizati0on of heat transport through biological media incorporating hyperthermia treatment. Int J Heat Mass Transf 2009;52:1608–18.
[35] Iasiello M, Vafai K, Andreozzi A, Bianco N, Tavakkoli F. Effects of external and internal hyperthermia on LDL transport and accumulation within an arterial wall in the presence of a stenosis. Ann Biomed Eng 2015;43:1585–99.